

Chiral Quirkonium Decays

R. Fok¹ and Graham D. Kribs^{2,1}

¹*Department of Physics, University of Oregon, Eugene, OR 97403*

²*Theoretical Physics Department, Fermilab, Batavia, IL 60510*

We calculate the two-body decay rates of “quirkonium” states formed from quirks that acquire mass solely through electroweak symmetry breaking. We consider $SU(N)_{ic}$ infracolor with two flavors of quirks transforming under the electroweak group (but not QCD) of the Standard Model. In one case, the quirks are in a chiral representation of the electroweak group, while in the other case, a vector-like representation. The differences in the dominant decay channels between “chiral quirkonia” versus “vector-like quirkonia” are striking. Several chiral quirkonia states can decay into the unique two-body resonance channels WH , ZH , $t\bar{t}$, $t\bar{b}/b\bar{t}$, and γH , which never dominate for vector-like quirkonia. Additionally, the channels WW , WZ , ZZ , and $W\gamma$, are shared among both chiral and vector-like quirkonia. Resonances of dileptons or light quarks (dijets) can dominate for some vector-like quirkonia states throughout their mass range, while these modes never dominate for chiral quirkonia unless the decays into pairs of gauge or Higgs bosons are kinematically forbidden.

I. INTRODUCTION

Quirks are fermions transforming under the SM gauge group along with a new strongly-coupled “infracolor” group $SU(N)_{ic}$ [1]. (Earlier ideas were also considered in Ref. [2].) The scale of infracolor confinement, Λ_{ic} , is assumed to be much smaller than the masses of all quirks, and so the infracolor-strings have an exponentially suppressed rate to break. Quirks pairs produced in a collider remain in a bound state even when produced with large kinetic energies. This leads to several interesting collider physics and dark matter applications [1, 3–14]. (Other work on hidden valley models can be found in [15–17].) Certain kinds of quirks have already been searched for at the Tevatron by the D0 collaboration [18].

In this paper, we are mainly interested in quirks that acquire mass through electroweak symmetry breaking. This is unlike the original model, Ref. [1], where quirks acquired “vector-like” masses independently of electroweak symmetry breaking. We are motivated in part by the discovery that chiral quirks bound in quirky baryons can lead to a viable asymmetric dark matter candidate [10]. We do not, however, restrict ourselves to the specific theory or detailed parameter choices of [10]. Instead, we consider general $SU(N)_{ic}$, and calculate the meson decay rates for both chiral quirks as well as vector-like quirks, demonstrating the experimentally distinguishable signatures.

At this point we should emphasize that only some aspects of quirky physics can be calculated (or simulated) with standard collider tools. In general, quirks can be produced in a standard collider physics process (for us, weak production), but then the p_T of the quirks must be shed before the quirks settle down into a low-angular-momentum state. This “spin-down” process is in general non-perturbative, with the resulting radiation dependent on the relative strengths of infracolor and other couplings of the quirks. After spin-down and energy loss, the constituent quirks annihilate, causing quirky mesons to decay. It is solely this last step that is our interest in this

paper.

The annihilation rate of quirky mesons is proportional to the lowest non-vanishing radial derivative of the meson wavefunction at zero relative quirk displacement. This is entirely analogous to positronium and quarkonium [19]. For an S state, this is $|\psi(0)|^2$, while for a P state, $|\psi'(0)|^2$. At high orbital angular momentum L , this wavefunction factor is suppressed. Ref. [1] estimated the suppression factor in the annihilation probability scaling as $(\beta/L)^{L+1}/L$, where β is the quirk relative velocity and $L > 0$. Therefore, instead of annihilating immediately, the quirky bound states are expected to emit soft radiation to shed their angular momentum.¹ As the quirky bound state reaches a low angular momentum state ($L \sim 1$), the constituent quirks ultimately annihilate; some quirky meson decay rates for certain vector-like quirks have been discussed in [1, 3, 4, 14].

This paper is organized as follows. We will describe our quirk model in Sec. II. Next, we present a qualitative understanding of the parametric dependencies of the various decay channels in Sec. III. We present the formalism to calculate the decay amplitudes in Appendix A, along with the extensive analytical results for all of our quirkonia decay rates in Appendices B and C. Much of our results for neutral quirkonia can be obtained from earlier results on heavy quarkonium [19], which we have compared extensively. Then, we present numerical evaluations of our results, and discuss their implications, in Sec. IV. Next, we calculate the decay rates for vector-like quirkonia in Sec. V, comparing and contrasting to the chiral quirkonia decay results. We summarize and provide a clear explanation of which modes have “chiral enhancement” in Sec. VI. We conclude with a discussion, identifying the major signals that distinguish chiral quirkonia from vector-like quirkonia in Sec. VII.

¹ The radiation may be in the form of soft photons [5] that can be detected as rings in the $\eta - \phi$ plane in colliders.

	$SU(N)_{ic}$	$SU(2)_L$	$U(1)_Y$
Q	\mathbf{N}	$\mathbf{2}$	0
u^c	$\bar{\mathbf{N}}$	$\mathbf{1}$	$-1/2$
d^c	$\bar{\mathbf{N}}$	$\mathbf{1}$	$+1/2$

TABLE I: Quirk quantum numbers.

II. MODEL AND SETUP

The model we consider is $SU(N)_{ic}$ with two flavors in the representations given in Table I. This is the generalization of the model of Ref. [10] to N infracolors. We assume $\Lambda_{ic} \ll m_Q$, and neglect the infracolor confinement contribution to the quirky meson masses. The Lagrangian that gives mass to the quirks is simply

$$\mathcal{L} = \lambda_U Q H u^c + \lambda_D Q H^\dagger d^c. \quad (1)$$

Despite the abuse of notation (Q , u^c , d^c), we emphasize that our quirks are color *singlets*. After electroweak symmetry breaking, the quirks acquire masses $M_{U,D} \equiv \lambda_{U,D} v$. Writing the electroweak doublet as $Q = (u, d)$, we can write the quirks in terms of four-component Dirac spinors U, D

$$U = \begin{pmatrix} u \\ u^{c\dagger} \end{pmatrix} D = \begin{pmatrix} d \\ d^{c\dagger} \end{pmatrix} \quad (2)$$

where U, D have electric charge $q = \pm 1/2$. The quirky mesons formed from these objects include

$$(U\bar{U}), (D\bar{D}) \quad \text{neutral mesons} \quad (3)$$

$$(U\bar{D}), (D\bar{U}) \quad q = \pm 1 \text{ charged mesons}. \quad (4)$$

There are two interesting regions of parameter space satisfying the requirement $\Lambda_{ic} \ll M_{U,D}$. One occurs when one quirk mass is much heavier than the other, $M_U \gg M_D$ or $M_D \gg M_U$, such that there is one set of heavy neutral mesons, one set of intermediate-mass electrically charged mesons, and one of set of light mesons. In this regime, the heavier mesons generically weak decay to the lightest mesons (microscopically the heavier quirks are weak decaying into the lighter quirks) *before* the quirks themselves have time to annihilate. In this regime, the relevant annihilation channels consist solely of the lightest neutral mesons.

The second regime, and the main focus of this paper, is when $M_U \simeq M_D$. When the two flavors of quirks are very nearly degenerate in mass, all of the mesons given in Eqs. (3),(4) are virtually stable against weak decay. All of the quirk pairs within the mesons therefore annihilate well before the kinematically-suppressed weak decay occurs. This leads to four distinct “towers” of mesons: two sets of neutral mesons and two sets of (oppositely) charged mesons.

The neutral mesons ($U\bar{U}$) and ($D\bar{D}$) can mix with each other through infragluon box diagrams that are superficially similar to the W -box diagrams within the SM that

lead to mixing among the neutral mesons of QCD. However, unlike QCD, all of the quirks are heavy, while the gauge bosons being exchanged in the box diagram are massless. This small mixing is an interesting effect for further study. Our meson decay rates are invariant under $U \leftrightarrow D$, and we simply compute $(Q\bar{Q})$ as if it were an exact $(U\bar{U})$ or $(D\bar{D})$ eigenstate. In practice, there may be either a small admixture between these states, in which case the mixing angle cancels out in our branching ratio calculations, or otherwise for maximal mixing, we treat $(Q\bar{Q})$ as the $[(U\bar{U}) + (D\bar{D})]/\sqrt{2}$ eigenstate.

The quirkonium bound state confining potential in the Coulombic approximation is [10]

$$V(r) = -\frac{\bar{\alpha}}{r}, \quad (5)$$

where $\bar{\alpha}$ contains the relevant couplings for the quirks in our model. When infracolor dominates, this is given by $\bar{\alpha} \simeq \bar{\alpha}_{ic} \equiv C_2(\mathbf{N})\alpha_{ic} = (N^2 - 1)/(2N)\alpha_{ic}$. The decay widths are proportional to the meson wavefunction when the two constituent quirks overlap. The wavefunction factors that appear in the decay widths, for S and P states are

$$|R_S(0)|^2 = 4 \left(\frac{1}{4} \bar{\alpha}_{ic} M \right)^3 \quad (6)$$

$$|R'_P(0)|^2 = \frac{1}{24} \left(\frac{1}{4} \bar{\alpha}_{ic} M \right)^5, \quad (7)$$

where M is the mass of the meson of the appropriate quirkonia state.

Implicit in evaluating the wavefunctions, Eqs. (6),(7), we have assumed the binding energy is dominated by the contributions from the infracolor interaction. This is *not* assumed by our analytic results, which are written in terms of the radial wavefunction at the origin. Moreover, since our numerical results are concerned with *ratios* of decay rates, the dependence on the wavefunction completely drops out of the S state quirkonia decay rates, and is not particularly sensitive for P states, as we will see.

Transitions between principal quantum numbers can occur, just as in bound state problems of QED. The transition between the $n = 2$ P states to the $n = 1$ S states is given by the Lyman-alpha electromagnetic transition rate. This was estimated for neutral quirkonia to be [10]

$$\Gamma_{L-\alpha} = \frac{4}{9} e_Q^2 \alpha_{em} E_{L\alpha}^3 |\langle 0|r|1 \rangle|^2 = \frac{1}{4} \left(\frac{8}{81} \right)^2 \alpha_{em} \bar{\alpha}_{ic}^4 M, \quad (8)$$

where M is roughly the meson mass. Charged quirkonia have the same rate, so long as infracolor dominates the potential, Eq. (5). As we will see, the Lyman-alpha transition is typically faster than the annihilation rates of P state quirkonia. There are exceptions, however, for chiral quirkonia, which we calculate below, and discuss the resulting final state signatures.

III. QUALITATIVE DESCRIPTION OF RESULTS

The formalism we used for our quirkonia decay calculations is given in Appendix A, and the complete analytic results are given in Appendices B and C. Here, we evaluate the parametric scaling of the various transition and decay rates. There are five qualitatively distinct rates involved in quirkonia decay:

$$\Gamma_{L-\alpha}(P \rightarrow S) \sim \alpha_{em} \bar{\alpha}_{ic}^4 M \quad (9)$$

$$\Gamma(S \rightarrow g'g') \sim \bar{\alpha}_{ic}^5 M \quad (10)$$

$$\Gamma(S \rightarrow \text{SM} + \text{SM}) \sim \alpha_{\text{SM}}^2 \bar{\alpha}_{ic}^3 M \left(\frac{M^2}{m^2} \right)^\beta \quad (11)$$

$$\Gamma(P \rightarrow g'g') \sim \bar{\alpha}_{ic}^7 M \quad (12)$$

$$\Gamma(P \rightarrow \text{SM} + \text{SM}) \sim \alpha_{\text{SM}}^2 \bar{\alpha}_{ic}^5 M \left(\frac{M^2}{m^2} \right)^\beta \quad (13)$$

The first rate corresponds to the Lyman-alpha electromagnetic transition given by Eq. (8) above. The second rate, $S \rightarrow g'g'$ refers to specifically the 1S_0 state decaying into a pair of infragluons. Note that the 3S_1 quirkonia state does not decay into a pair of massless gauge bosons, due to angular momentum conservation, just like the 3S_1 quarkonia state [19]. The third rate, $S \rightarrow \text{SM} + \text{SM}$ refers to 1S_0 or 3S_1 state decaying into a pair of SM particles with SM coupling α_{SM} . The fourth and fifth rates, $P \rightarrow g'g'$ and $P \rightarrow \text{SM} + \text{SM}$, refer to any of the P states decaying into the above modes. Generally, if the Lyman-alpha transition is possible (i.e., for any of the P states), it dominates over the quirkonia decay modes. The exception to this is if there is longitudinal or Yukawa “chiral enhancement”, which can occur either singly ($\beta = 1$) or doubly ($\beta = 2$) depending on the final state. Double-longitudinal enhancement tends to overcome Lyman-alpha emission when M is somewhat larger than one of the SM bosons, $m = M_W, M_Z$, compensating for the suppression by the larger number of couplings. Calculating exactly which modes are enhanced, and why, is the main thrust of the paper.

The residual dependence of the decay branching ratios on the parameters of the theory, α_{ic} , Λ_{ic} , and the infracolor group $SU(N)_{ic}$, arise from: a) neutral quirkonium decay into infragluons, b) possible Lyman-alpha infragluon transition, and c) Lyman-alpha electromagnetic transition.

The first issue, neutral quirkonium decay into infragluons, is handled by choosing to evaluate “width ratios” into visible SM particles, rather than the standard branching ratios of neutral quirkonium decays. This is because the infragluons are expected to be very long-lived and escape the detector [1], and thus annihilation to $g'g'$ is expected to yield no hard SM resonance signal. The possibility of 3-body decays, going into a pair of infragluons as well as a SM particle, is beyond the scope of this paper.

The second issue, Lyman-alpha infragluon transi-

tion, can occur if the kinematics of the transition permit it. The energy difference between the $n = 2$ P state and the $n = 1$ S state is $(3/32)\bar{\alpha}_{ic}^2 M$. The infragluon mass is of order, but somewhat larger than Λ_{ic} . For $\bar{\alpha}_{ic} \sim O(0.1)$ and $\Lambda_{ic} \sim O(1 \text{ GeV})$, the infragluon mass is already close to this energy splitting, and so kinematic suppression is generic for somewhat larger values of $\bar{\alpha}_{ic}$. For smaller values of Λ_{ic} , presumably accompanied by smaller values of $\bar{\alpha}_{ic}$, the infragluon emission is less kinematically suppressed but has an overall transition rate that is smaller. In this region of small $\bar{\alpha}_{ic}$, the P states are more likely to transition to S states before annihilating. A different choice of the infracolor group introduces an order one change to $\bar{\alpha}_{ic}$, as well as the running of $\bar{\alpha}_{ic}$ in the Coulombic potential [10]. Since these changes appear as shifts in the coupling of the Coulombic potential, they can be at least partially absorbed by a redefinition of $\bar{\alpha}_{ic}$.

Finally, there is the different dependence on $\bar{\alpha}_{ic}$ (and α_{SM}) between the Lyman-alpha transition rate versus the quirkonia decay rates. The Lyman-alpha transition scales as $\alpha_{\text{SM}} \bar{\alpha}_{ic}^4$, whereas the decay rates of the P states scale as $\alpha_{\text{SM}}^2 \bar{\alpha}_{ic}^5$ through $|R'_P(0)|^2$. Hence, there is a relative suppression of branching and width ratios of roughly $\alpha_{\text{SM}} \bar{\alpha}_{ic}$ relative to the Lyman-alpha electromagnetic transition rate.

Consider two regimes, one in which the Lyman-alpha transition rate is dominant and the other where it is subdominant to decay rates that are doubly-enhanced. In the latter regime, the branching and width ratios are rather insensitive to $\bar{\alpha}_{ic}$, since the only dependence on $\bar{\alpha}_{ic}$ enters from the wavefunction. This dependence drops out, analogous to the S states. In the first regime, however, the total width is dominated by the Lyman-alpha transition rate. The width and branching ratios of decay processes scale linearly with $\bar{\alpha}_{ic}$. But, the regime where the potential is dominated by infracolor while still allowing a Coulombic approximation to the bound state potential only allows for about one order of magnitude change in $\bar{\alpha}_{ic}$.

IV. BRANCHING RATIOS AND WIDTH RATIOS

We now present our results for charged and neutral quirkonia decay rates. In what follows, we carry out several numerical computations of branching ratios and width ratios, using the results from Appendices B and C, to demonstrate the dominant SM decay channels for the various bound states of quirkonia.

In the following, we have chosen a specific infracolor group, $N = 2$, and infracolor coupling, $\bar{\alpha}_{ic} = 0.2$. As we discussed above, the additional relative suppression factor of the P state decay rates is only one power of $\bar{\alpha}_{ic}$. The value $\bar{\alpha}_{ic} = 0.2$ tends to maximize the possibility that P states can, at larger quirkonium masses, annihilate into SM modes before the Lyman-alpha transition

occurs.

A. Charged quirkonia

We now discuss the branching ratios of charged quirkonia. The analytic results for the decay rates can be found in Appendix B. Given a final state f , the branching ratio for f , $BR(Q\bar{Q} \rightarrow f)$, is

$$BR(Q\bar{Q} \rightarrow f) = \frac{\Gamma(Q\bar{Q} \rightarrow f)}{\sum_f \Gamma(Q\bar{Q} \rightarrow f)}, \quad (14)$$

where the sum is over all final states.

The charged quirkonium case is particularly simple. As the system is electrically charged, it cannot decay into $g'g'$. Fig. 1 shows the decay branching ratios of charged quirkonium states. For all states, only the WH partial width is sensitive to different values of the Higgs mass. The plots shown for charged quirkonia here are also applicable to any massive bound states that only decay via the electroweak $SU(2) \times U(1)$ group, with electric charges $Q_u = -Q_d = 1/2$. Note that we only show the summed width over the massless fermions (2 quark pairs, 3 lepton-neutrino pairs), as the widths of all massless fermions are the same (see App. B 4). Also, we only show the decays for the $U\bar{D}$ meson. We have checked that the widths for $\bar{U}D$ decay are the same.

The branching ratios of different bound states are plotted in Fig. 1. For the S states, the WZ partial width dominates. For P states, radiative transition usually dominates. For 3P_1 , the WH width becomes larger than the Lyman-alpha transition width when the meson mass is larger than $\gtrsim 600$ GeV, provided that the meson is heavier than the threshold.

B. Neutral Quirkonia

The results for neutral quirkonia are more complicated than their charged counterparts. Not only that there are more decay channels, but in some cases the mesons can decay into infragluon pairs, $g'g'$, that hadronize into an infragluon pair $\phi'\phi'$.

1. $g'g'$

As the mesons are color singlets, only t - and u -channels contribute to the decay amplitudes of $B \rightarrow g'g'$. Then the decay rate should be proportional to that of $B \rightarrow \gamma\gamma$. A simple calculation shows that, for an $SU(N)_{ic}$ color gauge group,

$$\Gamma(B \rightarrow g'g') = \frac{N^2 - 1}{4N^2} \frac{\alpha_{ic}^2}{e_Q^4 \alpha_{em}^2} \Gamma(B \rightarrow \gamma\gamma) \quad (15)$$

where e_Q is the quirk electric charge. Setting $N = 3$ reproduces the results in [19]. The 3S_1 state cannot decay into $g'g'$. Its decay into $g'g'g'$ is given by [4],

$$\Gamma({}^3S_1 \rightarrow g'g'g') = \frac{(N^2 - 1)(N^2 - 4)}{N^2} \frac{(\pi^2 - 9)\alpha_{ic}^3}{9\pi M^2} |R_S(0)|^2. \quad (16)$$

This vanishes for the special case $SU(2)_{ic}$, since three gluons cannot form a infracolor singlet.

Instead we present our results in terms of a “width ratio”

$$WR(Q\bar{Q} \rightarrow f) = \frac{\Gamma(Q\bar{Q} \rightarrow f)}{\sum_{f \neq \phi'\phi'} \Gamma(Q\bar{Q} \rightarrow f)}, \quad (17)$$

Also, for reasons of clarity, we do not present the plots for the branching ratios when the Higgs mass deviates from 125 GeV. Unless the final states involve Higgs bosons, a larger Higgs boson mass would only push the corresponding thresholds towards higher meson masses, leaving the other width ratios mostly unchanged as in the case of charged quirkonia. However, there is a qualitative change in the width ratios for the 3P_0 state when the Higgs mass is sufficiently large, which will be discussed below.

2. 1S_0 and 3S_1

The width ratios for the S states are shown in Figs. 2a-2b. The dominant decay channels are ZH and $t\bar{t}$. The ZH channel receives double enhancement from the longitudinal Z and the Yukawa coupling between the Higgs boson and the quirk. Also, the $t\bar{t}$ channel is enhanced by the top mass.

The results for the 3S_1 state can be discussed more precisely because the infragluon channel is absent. Even for values of M not far away from $2m_W$, the double longitudinal WW mode dominates. Because of Bose symmetry, the two Z 's cannot be longitudinal simultaneously and the ZZ mode is suppressed.

3. 1P_1

The width ratios are shown in Fig. 2d is dominated by the Lyman-alpha transition throughout the sub-TeV range. All other widths contain a single enhancement factor, from either the longitudinal mode or the quirky Yukawa.

4. 3P_0

The 3P_0 width ratios exhibit an interesting feature when the Higgs mass is larger than $2m_W$, $2m_Z$ and $2M_t$, where M_t is the top mass. The decay channels WW , ZZ , and $t\bar{t}$ involves an s -channel Higgs boson exchange. When the meson mass is near the Higgs mass $M \sim M_H$,

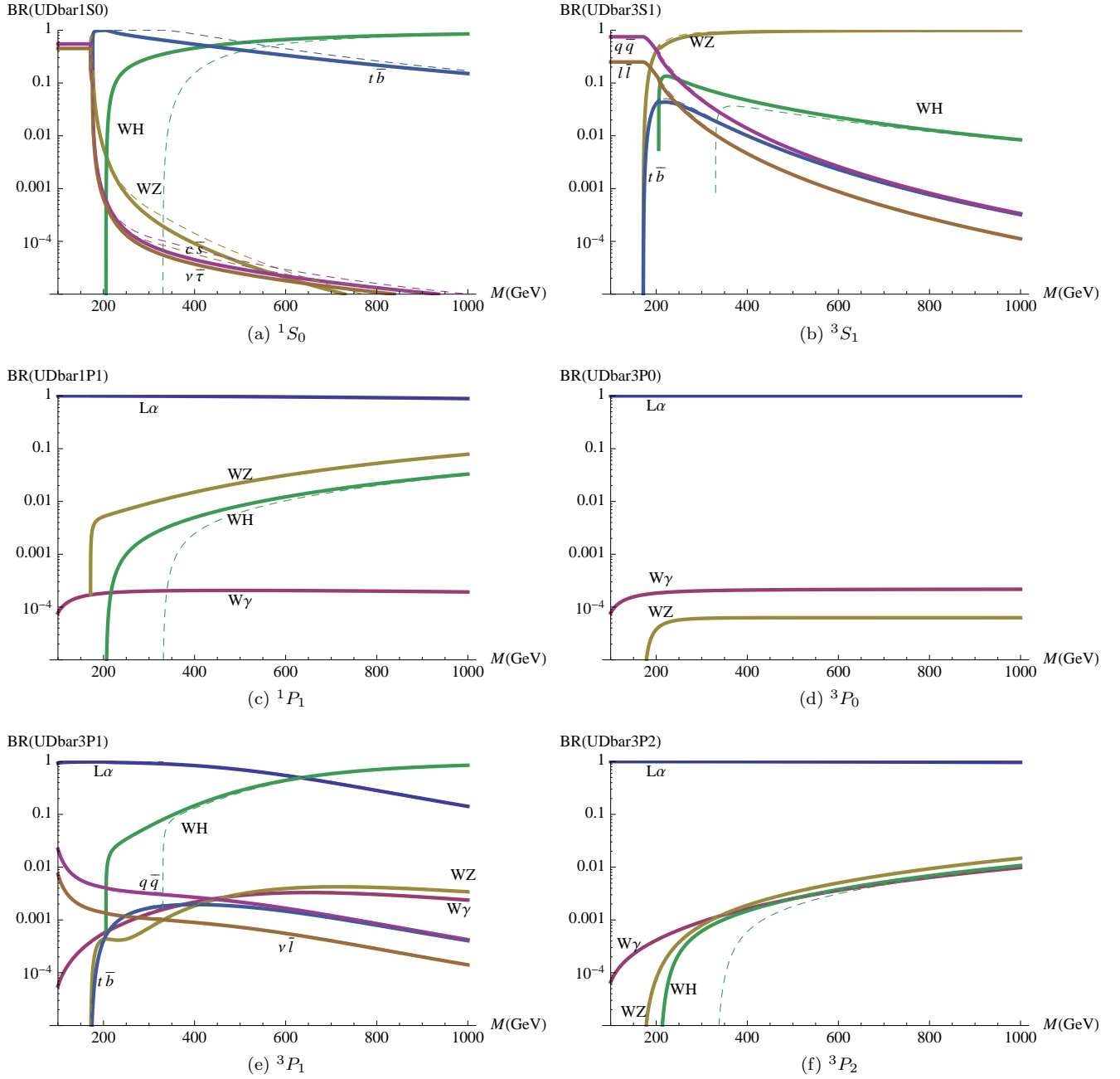


FIG. 1: Decay branching ratios of charged chiral quirkonia in different J^{PC} states. Solid lines are with Higgs mass $M_H = 125$ GeV, dashed lines with $M_H = 250$ GeV.

the widths are enhanced by the s -channel Higgs resonance. This can be seen in Fig. 3. There, the WW and ZZ widths have a resonance at $M = M_H = 250$ GeV when the s -channel Higgs boson is on-shell. The $t\bar{t}$ width does not exhibit this behavior because at 250 GeV, the decay into two top quarks from a single Higgs boson is kinematically forbidden.

5. 3P_1

The branching ratios for the 3P_1 state are shown in Fig. 2e. The ZH channel are doubly enhanced and is dominant for $M \gtrsim 700$ GeV.

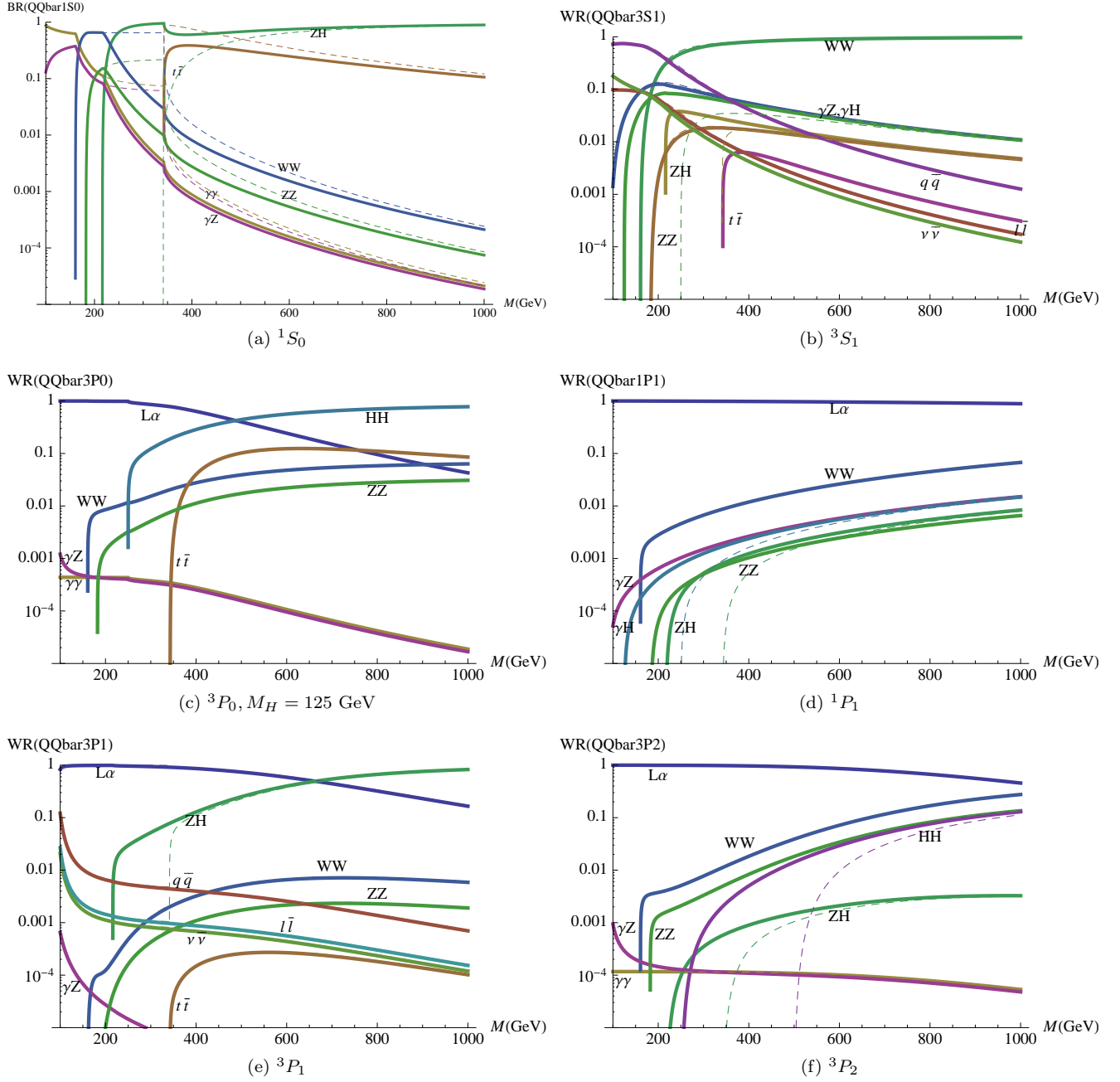


FIG. 2: Decay width ratios of neutral chiral quirkonia in different J^{PC} states. Solid lines correspond to a Higgs mass $M_H = 125$ GeV, while dashed lines correspond to $M_H = 250$ GeV. In many instances, there is no difference between the width ratios for different Higgs masses, and thus the solid lines overlap the invisible dashed lines. For figure (c), we have presented the choices $M_H = 125$ GeV. We illustrate the difference in decay width ratios changing to $M_H = 250$ GeV in Fig. 3.

6. 3P_2

The channels WW , ZZ and HH are doubly enhanced and will take over the radiative transition at high meson mass ($\gtrsim 1$ TeV).

V. COMPARISON TO VECTOR-LIKE QUIRKONIA

Annihilation rates for the case of vector-like quirks in certain other representations has been calculated in [4, 13]. There is not a general rule that relates the decay rates of vector-like quirks to chiral quirks. But in certain

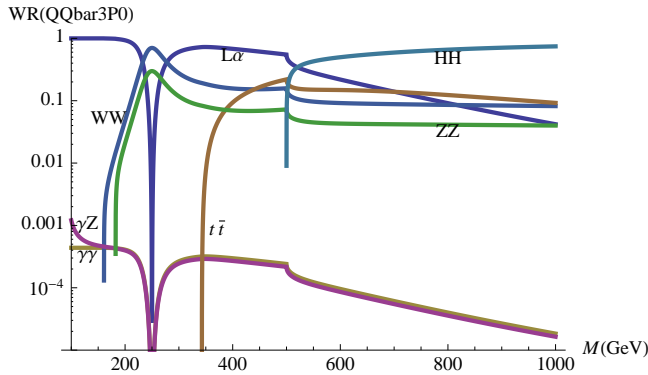


FIG. 3: 3P_0 with $M_H = 250$ GeV. The resonance structure is due to the s -channel Higgs boson.

circumstances one can be obtained from the other, and vice versa. In this section, we will discuss differences and similarities of vector-like and chiral quirk decay rates, and give examples in cases where the decay rates are related.

We wish to compare our results for chiral quirks to a related theory with vector-like quirks. The vector-like theory we consider consists of the doublet Q given before in Table I, but now we replace

$$\begin{bmatrix} u^c(\bar{\mathbf{N}}, \mathbf{1}, -1/2) \\ d^c(\bar{\mathbf{N}}, \mathbf{1}, +1/2) \end{bmatrix} \rightarrow Q'(\bar{\mathbf{N}}, \mathbf{2}, 0). \quad (18)$$

Yukawa couplings, Eq. (1), are not present, and instead we write the vector-like mass MQQ' where $M = M_U = M_D$. There are several differences that lead to qualitatively different decay widths.

First, the coupling of electroweak gauge bosons to left- and right-handed quirks are the same – the quirk- W/Z coupling is a purely vector interaction, and processes that proceed through the axial vector coupling in the chiral case are absent for vector-like quirks. As an example, consider the decay rate $\Gamma({}^3S_1 \rightarrow f\bar{f})$, for neutral and charged quirkonia. The only diagrams are the s -channel γ/Z or W . In the neutral case, the only difference that separates vector-like and chiral is the different axial-vector and vector coupling of the Z . Therefore, the expressions for vector-like [4] and chiral [19] are the same. For the charged case, the axial-vector and vector couplings are not explicitly written in [4], but their rate is 4 times larger than the chiral case in [19]. This is because the s -channel W couples to both left and right handed quirks in the vector-like case, whereas in the chiral case they only couple to left handed quirks. Therefore, the decay rate into a fermion-antifermion pair for a charged 3S_1 is four times larger than its chiral counterpart.

Second, the quirks do not couple to the Higgs and the corresponding Goldstone bosons (through the longitudinally polarized electroweak gauge bosons). Virtual Goldstone bosons can only appear in the s -channel, and since the Goldstone bosons are pseudoscalars, they only contribute to the 1S_0 decay rates. Vector-like quirks,

by contrast, do not have couplings to the Higgs or the Goldstone bosons. In addition, Goldstone bosons can appear in the final state (appearing as longitudinally polarized electroweak gauge bosons). This leads to qualitatively different decay rates into gauge bosons for all of the bound states.

For completeness, we present the width and branching ratios of vector-like quirkonia in Fig. 4 for neutral quirkonia and Fig. 5 for charged. There are striking differences between the chiral and vector-like cases. The most prominent feature in the vector-like case is that all decay widths have the same asymptotic behavior at large quirkonium mass – there are no longitudinal enhancements of W/Z anywhere. This is expected, as the longitudinal W/Z asymptotes to the respective Goldstone bosons, which do not couple to the vector-like quirks in u - and t -channel quirk-exchange diagrams. Also, the trilinear gauge boson coupling appearing in s -channel gauge boson exchange arises from the electroweak gauge structure of $SU(2)_L$ and has no relation to the electroweak breaking mechanism. Therefore, one would not expect any enhancements in the decay widths of vector-like quirkonia. Without longitudinal enhancements, the Lyman-alpha transition dominates over all P -state decays for all quirkonium masses. Whereas in the chiral case, decay channels that receives longitudinal enhancements can dominate the Lyman-alpha transition at large quirkonium masses.

In the low quirkonium mass regime, the overall behavior of both vector-like and chiral quirkonia are similar: P -states predominantly decay via the Lyman-alpha transition and 3S_1 into $q\bar{q}$. It is interesting to note that for 1S_0 , γZ dominates the vector-like quirkonium decay, whereas $\gamma\gamma$ is dominant for chiral quirkonia. This is because the primordial electroweak gauge boson W_3^μ couples not just to the left-handed vector-like quirk, but to the right handed one also! A rough estimate indicates that this gives a factor of four increase in the γZ rate for the vector-like case. Indeed, the isospin contribution to the vector coupling of the Z to the quirks for the vector-like case is twice as much as that for chiral quirks.

VI. UNDERSTANDING CHIRAL ENHANCEMENTS

Figures 1 and 2 show that decay processes can be singly or doubly enhanced by either the Yukawa coupling or the longitudinal modes of gauge bosons at high quirkonium masses. A summary of enhancements received in the decay channels can be found in Tables II and III. In this limit, the Goldstone equivalence theorem applies and the enhancements in various decay channels can be seen by the matching of the J, P , and C numbers between the decay quirkonium state and the final state consisting of Goldstone/Higgs bosons and/or transverse gauge bosons. First, we determine the J^{PC} numbers to the final state particles; 0^{-+} and 0^{++} to the Goldstone boson and Higgs boson, respectively. For photons and transverse W and

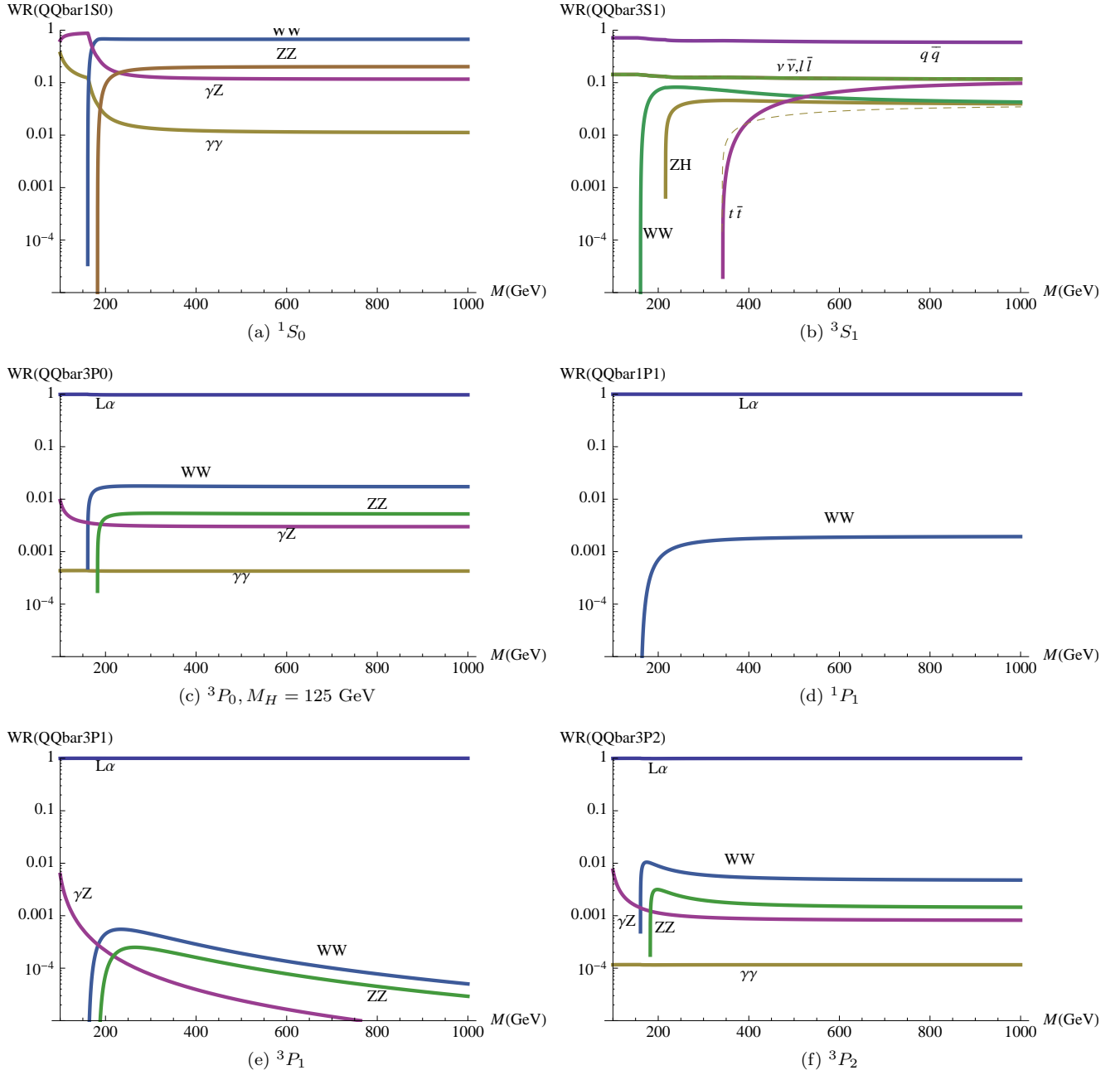


FIG. 4: Decay width ratios of neutral vector-like quirkonia in different J^{PC} states. Solid lines correspond to a Higgs mass $M_H = 125$ GeV, while dashed lines correspond to $M_H = 250$ GeV. In many instances, there is no difference between the width ratios for different Higgs masses, and thus the solid lines overlap the invisible dashed lines.

Z , we assign P and C numbers according to the P and C of the bilinears $\bar{\psi}\gamma^\mu\psi$ and $\bar{\psi}\gamma^\mu\gamma^5\psi$. The photon has $J^{PC} = 1^{--}$, and the W/Z has 1^{--} for the vector coupling and 1^{++} for the axial vector coupling (that is, we absorb the violation of C and P from the axial vector coupling into the J^{PC} of the W and Z). For the quirkonia, we have 0^{-+} for $1S_0$, 1^{--} for $3S_1$, 1^{+-} for $1P_1$, 0^{++} for $3P_0$, 1^{++} for $3P_1$ and finally, 2^{++} for $3P_2$.

Next, we write down all the available J^{PC} with differ-

ent orbital angular momentum L between the two final state particles, and match with the J^{PC} of the quirky meson to determine which meson decay channels are enhanced. As an example, consider $\bar{Q}Q \rightarrow Z\gamma$, where there are only the t - and u -channel diagrams. Single enhancement from the longitudinal Z is present in some meson states. In the limit where the quirkonium mass $M \gg M_Z$, the longitudinal Z is equivalent to the corresponding Goldstone boson ϕ^0 . The J^{PC} of the $\phi^0\gamma$ sys-

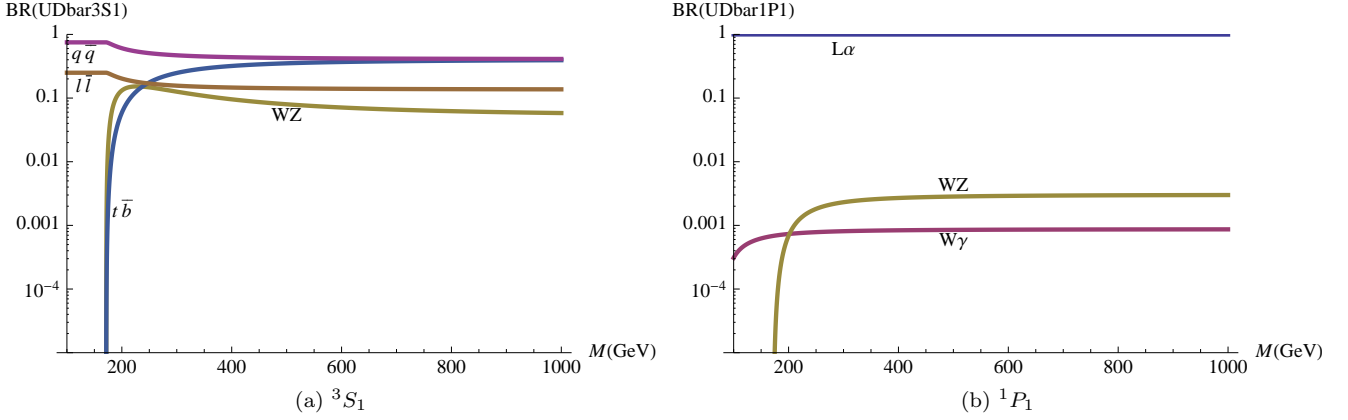


FIG. 5: Same as Fig. 4 but for charged vector-like quirkonia. Only the two J^{PC} states shown here have nontrivial branching ratios. The state 3S_1 cannot decay through two-body decays. The $^3P_{0,1,3}$ states can only decay radiatively into S states.

J^{PC}	Singly enhanced	Doubly enhanced
1S_0		WH
3S_1	$W\gamma, WH, WZ$	
1P_1	$W\gamma, WH, WZ$	
3P_0		
3P_1	$W\gamma, WZ$	WH
3P_2	$W\gamma, WH, WZ$	

TABLE II: Decay channels that receive enhancements for charged quirkonia.

J^{PC}	Singly enhanced	Doubly enhanced
1S_0		ZH
3S_1	$Z\gamma, ZZ, ZH, \gamma H$	WW
1P_1	$Z\gamma, WW, ZZ, ZH, \gamma H$	
3P_0		WW, ZZ, HH
3P_1	$Z\gamma, WW, ZZ$	ZH
3P_2	$Z\gamma, ZH$	WW, ZZ, HH

TABLE III: Decay channels that receive enhancements for neutral quirkonia.

tem is determined by combining that of the Goldstone boson (0^{-+}) and that of the photon 1^{--} , which gives 1^{+-} . Keeping the total angular momentum $J \leq 2$, we can add orbital angular momentum L into the system, forming $\{0^{--}, 1^{--}, 2^{--}\}$ for $L = 1$, and $\{1^{+-}, 2^{+-}\}$ for $L = 2$. This is captured in Table IV. One sees that, only the states 1^{+-} and 1^{--} matches with the existing quirky meson states 1P_1 and 3S_1 , respectively. One can see from Appendix C 2, that only the 1P_1 and 3S_1 states are enhanced. One can also see that both of the decay proceed via the axial vector coupling of the Z . This is because the $\phi^0 f f$ coupling is a pseudoscalar coupling $\bar{\psi}\gamma^5\psi$, and this must correspond to the axial vector coupling of the

	$J = 0$	$J = 1$	$J = 2$
$L = 0$		1^{+-}	
$L = 1$	0^{--}	1^{--}	2^{--}
$L = 2$		1^{+-}	2^{+-}

TABLE IV: J^{PC} of the $\phi^0\gamma$ system.

	$J = 0$	$J = 1$	$J = 2$
$L = 0$	0^{++}	1^{++}	2^{++}
$L = 1$	0^{-+}	1^{-+}	2^{-+}
$L = 2$		1^{++}	2^{++}

TABLE V: J^{PC} of the $Z_T\gamma$ system with vector coupling of the Z .

$Z, \bar{\psi}\gamma^\mu\gamma^5\psi$.

We will go further and illustrate that all other meson states decay to $Z\gamma$ via the vector coupling and receive no enhancements with the same procedure. Consider the final state with a transverse Z and γ , both with $J^{PC} = 1^{--}$ for the vector coupling of the Z . The J^{PC} of the final states are collected in Table V, where one can see that the $^1S_0, ^3P_0, ^3P_1$, and the 3P_2 states are not enhanced. The J^{PC} of the final states with an axial vector coupling can be obtained by flipping the C and P numbers everywhere in Table V. Then one sees that there are also contributions with no longitudinal Z enhancements via the axial vector coupling to the decay widths of 3S_1 and 1P_1 . Indeed, there are terms in the expressions for the corresponding decay widths that are not enhanced.

The procedure above can explain a large number of enhancements for different quirkonium decay processes. However, there are instances where the procedure predicts leading enhancements in some processes when there should not have been any. The fictitious leading enhancements predicted by this procedures are: $^1S_0 \rightarrow W_T^-\phi^+$,

$^1S_0 \rightarrow \phi^+\gamma$, $^1P_1 \rightarrow \phi^+H$, $^3P_0 \rightarrow W_T^+H$ and $\{^1S_0, ^3P_0\} \rightarrow Z_T\phi^+$.

The 1S_0 state are not singly enhanced in two-body systems consisting of one transverse gauge boson. This can be seen by tracking the spin along the quirky fermion line. First, the 1S_0 projector is proportional to $\sum_{s_1 s_2} C_{^1S_0}^{s_1 s_2} u_{s_1} \bar{u}_{s_2}$, where $C_{^1S_0}^{s_1 s_2}$ is the Clebsh-Gordon coefficients corresponding to the 1S_0 state, which vanishes for $s_1 = s_2$. In the systems being considered, there is only one vertex that flips the spin - the fermion-fermion-gauge boson vertex. The rest are either scalar (Higgs boson) or pseudoscalar (Goldstone boson) couplings that do not involve a spin flip. Also, one can see that the Dirac spinor v has an opposite spin compared to the Dirac spinor u in the relation $v_s = -2s\gamma^5 u_{-s}$. Therefore, the 1S_0 state cannot decay into any states consisting of only one transverse gauge boson (with the other outgoing particle being the Higgs or Goldstone boson) and the 1S_0 decay width cannot be singly enhanced.

VII. DISCUSSION

We have calculated the chiral quirkonium decay rates for quirks that acquire mass through interactions with the Higgs boson. While in this paper we have not studied the production rates of quirks at the LHC, this is straightforward using standard collider physics tools, and has been done recently in the literature. For vector-like quirks with electroweak quantum numbers, the production cross section was calculated in Fig. 6 of Ref. [13]. There it was shown that pair production of uncolored quirks produced through γ/Z exchange has a cross section ranging from roughly $\sim 10^5$ to ~ 10 fb at $\sqrt{s} = 7$ TeV LHC for the quirkonium mass range of 100 to 1000 GeV. We expect that the chiral quirk production cross sections are very similar in size. Given the spectacular signals that result from quirkonia decay, the discovery of quirkonium resonances can occur quickly. This is likely to occur well before the detailed properties (spin, P , C , etc.) of the resonances can be determined.

The particular decay channels not only can tell us about the constituent quirks' quantum numbers, but perhaps even more interestingly, how the quirks acquire mass. Quirkonia with chiral quirks have longitudinal and Yukawa enhancements that are absent or highly suppressed in quirkonia with vector-like quirks. In this paper we have demonstrated the striking differences between the dominant chiral quirkonium decay channels as compared with vector-like quirkonium decay channels. This should enable the LHC to easily distinguish whether quirks are chiral or vector-like from the observation and branching ratios of the dominant decay channels.

For electrically-charged chiral quirkonia composed of quirks with the quantum numbers given in this paper, the state 1S_0 decays into WH or $t\bar{b}/\bar{t}b$ overwhelmingly

for quirkonium masses larger than about 250 GeV. Contrast this with vector-like quirkonia, where the 1S_0 with the quantum numbers given earlier in the paper, does not even have two-body decays. Chiral quirkonia in the 3S_1 state have WZ is the dominant decay channel. For vector-like quirkonia, the $f\bar{f}$, summed over all flavors of SM fermions, dominates. We also demonstrated that the Lyman-alpha transition is dominant in all of the charged quirkonia P -states, except for 3P_1 for chiral quirkonia when the “doubly-enhanced” WH decay becomes significant for quirkonium masses $\gtrsim 600$ GeV. The $W\gamma$ decay deserves more discussion. It was shown in [3] that the $W\gamma$ channel is dominant when their squirk and anti-squark pair has low relative velocity, in other words, an S -state. For our case, the $W\gamma$ partial width vanishes due to our choice of quantum numbers: $Q_U = -Q_D = 1/2$, where we found the $W\gamma$ partial width is proportional to $(Q_U + Q_D)^2$, see Appendix B 1.

For electrically-neutral chiral quirkonia, the dominant decay channels of 1S_0 are ZH and $t\bar{t}$. Again, contrast this with vector-like quirkonia where WW or ZZ dominates. For 3S_1 , the WW channel dominates for chiral quirkonia, versus $f\bar{f}$ for vector-like quirkonia. For all P -states, Lyman-alpha emission dominates for vector-like quirkonia, whereas for chiral quirkonia there are several decay channels that can become significant when the quirkonium mass is large. In particular, HH can dominate for 3P_0 , ZH for 3P_1 , and WW for 3P_2 .

Indeed, perhaps one of the most interesting decay channels that we found is the 3P_0 decay into two Higgs bosons, which becomes the dominant decay channel for quirkonium masses $\gtrsim 500$ GeV. This could be striking signal at LHC, given that the di-Higgs system would reconstruct to an invariant mass peak of the 3P_0 state.

Finally, it is tempting to consider applications of our results to various existing hints at colliders. For instance, the prominence of the electrically-charged chiral quirkonium decay channel, $^1S_0 \rightarrow WH$ is suggestive: chiral quirkonia with mass $M \sim 300$ GeV with some minor modification of the H decay into jets could easily lead to the CDF excess in the Wjj signal [21, 22]. The cross section can be easily adjusted to match the excess, simply by enlarging the number of infracolors or flavors of quirks. Given the incredible performance of the LHC over the past several months, we leave this pursuit to future work.

ACKNOWLEDGMENTS

We thank Z. Chacko, R. Harnik, and A. Martin for many useful discussions. GDK was supported by a Ben Lee Fellowship from Fermilab. RF and GDK were supported in part by the US Department of Energy under contract number DE-FG02-96ER40969 and by NSF under contract PHY-0918108. Fermilab is operated by Fermi Research Alliance, LLC, under Contract DE-AC02-07CH11359 with the US Department of Energy.

Appendix A: Matrix elements of bound state decays

This section reviews the procedures to evaluate the decay amplitudes of different angular momentum bound states following the method in [20]. We work in the non-relativistic limit, where the relative momentum of the constituents, $|\mathbf{q}| \ll M$, where M is the mass of the meson. We also ignore the contribution to the meson mass from the binding potential, i.e., we take $M = 2m_Q$, with m_Q the mass of the individual quarks.

Calculations of the matrix element involving an incoming bound state and an outgoing free state, $\langle X|iT|B \rangle$, are needed to evaluate different bound state decay rates. This is most conveniently done by writing the bound state as a superposition of free fermion states with spins (s_1, s_2) and momenta (p_1, p_2) :

$$\begin{aligned} |B\rangle &= |^{2s+1}l_j\rangle = \sum_{MS_z} \langle lms_{sz}|jj_z\rangle |lms_{sz}\rangle \\ &= \sqrt{\frac{2}{M}} \int \frac{d^3\mathbf{q}}{(2\pi)^3} \sum_{ms_z} \psi^{lm}(\mathbf{q}) \langle lms_{sz}|jj_z\rangle \times \\ &\quad \left[\sum_{s_1 s_2} \langle s_1, \frac{1}{2}, s_2, \frac{1}{2} | ss_z \rangle \right] |s_1 p_1 s_2 p_2\rangle, \end{aligned} \quad (\text{A1})$$

where ψ is the Schrödinger wavefunction of the bound state. In its rest frame, $p_1 = Q/2 + q$, and $p_2 = Q/2 - q$, where Q is the 4-momentum of the meson, and q is the relative 4-momentum of quarks. Then, the quantity $\langle X|iT|s_1 p_1 s_2 p_2 \rangle = i\bar{v}_{s_2}(p_2) \mathcal{M} u_{s_1}(p_1)$ is the usual fermion-antifermion annihilation matrix element into the outgoing state f . Expanding the above to the lowest non-vanishing order in \mathbf{q} , we found the following decay amplitudes for S and P states,

$$A(^1S_0) = \sqrt{\frac{N}{16\pi M}} R_S(0) \text{Tr}[\mathcal{M} \gamma^5 (-\not{Q} + M)], \quad (\text{A2})$$

$$A(^3S_1) = \sqrt{\frac{N}{16\pi M}} R_S(0) \text{Tr}[\mathcal{M} \not{\epsilon} (-\not{Q} + M)], \quad (\text{A3})$$

$$A(^1P_1) = -i \sqrt{\frac{3N}{4\pi M}} R'_P(0) \text{Tr}[\frac{1}{2} \epsilon_\mu \mathcal{M}^\mu \gamma^5 (-\not{Q} + M) + \mathcal{M} \not{\epsilon} \frac{\not{Q}}{M} \gamma^5], \quad (\text{A4})$$

$$A(^3P_0) = i \sqrt{\frac{N}{4\pi M}} R'_P(0) \text{Tr}[\frac{1}{2} \mathcal{M}^\alpha \left(\frac{Q_\alpha \not{Q}}{M^2} - \gamma_\alpha \right) (-\not{Q} + M) - 3\mathcal{M}], \quad (\text{A5})$$

$$A(^3P_1) = i \sqrt{\frac{3N}{8\pi M}} R'_P(0) \text{Tr}[2\mathcal{M} \not{\epsilon} \gamma^5 - \frac{i}{2M} \epsilon^{\rho\alpha\beta\delta} Q_\rho \mathcal{M}_\alpha \gamma_\beta \epsilon_\delta (-\not{Q} + M)], \quad \text{and} \quad (\text{A6})$$

$$A(^3P_2) = -i \sqrt{\frac{3N}{4\pi M}} R'_P(0) \text{Tr}[\frac{1}{2} \mathcal{M}_\alpha \epsilon^{\alpha\beta} \gamma_\beta (-\not{Q} + M)], \quad (\text{A7})$$

where $R(0)$ and $R'(0)$ are the meson radial wavefunction and its derivative at the origin, respectively.

The mass of each meson is distinct, and in principle the M in each of the above expressions should be replaced with the mass for that particular bound state. Since we assume $\bar{\alpha}_{ic}$ is perturbative, the differences between bound state energies is parametrically small, of order $\bar{\alpha}_{ic}^2 M$. In most instances, one can use our expressions below, substituting the proper quirkonia mass for M , and computing the rates. For the branching ratio plots we present below, however, this difference is small.

The quantity $\mathcal{M}_\alpha = \partial \mathcal{M} / \partial q^\alpha$ is the derivative of the matrix element with respect to the relative momentum q . The meson polarizations in the rest frame, ϵ^μ for spin-1, and $\epsilon^{\mu\nu}$ for spin-2, are chosen to be

$$\begin{aligned} \epsilon_{\mp}^\mu &= (0, \mp \frac{1}{\sqrt{2}}, -\frac{i}{\sqrt{2}}, 0), \\ \epsilon_L^\mu &= (0, 0, 0, 1), \\ \epsilon_{J_z}^{\alpha\beta} &= \sum_{M, S_z} \langle 1M, 1S_z | 2J_z \rangle, \end{aligned} \quad (\text{A8})$$

with $J_z \in \{-2, -1, 0, 1, 2\}$. The factor of \sqrt{N} arises from normalizing the meson as an infracolor singlet, exactly analogous to what is done with the QCD color factor for quarkonia [19].

The P and C parities of the above angular momentum states are manifest in each of the decay amplitudes above. For example, with $Q^\mu = (M, 0, 0, 0)$ in the rest frame, the P and C parities of the bilinear constructed from the

projector appearing in $A(^1S_0)$, $\bar{\psi}\gamma^5(-\not{Q} + M)\gamma^0\psi$, are $-$ and $+$, respectively. Thus $J^{PC} = 0^{-+}$ for 1S_0 , as expected. One can check that the other amplitudes give the expected J^{PC} using the same procedure. From Eqs. (A2) to (A7), we rederived all of the two-body decay rates listed in [19].²

Appendix B: Decay Rates of Charged Quirkonia

Apart from a color factor of N , decay rates of neutral quirkonia that do not involve any gluons are the same as listed in [19]. The decay rates of charged quirkonia will be discussed in this section.

Charged quirkonia are expected to have larger partial widths than their neutral counterparts. This is because charged particles do not have a well-defined charge conjugate parity, hence loosening the constraints posed by CP conservation. Here, we list the partial widths of charged quirky mesons with positive unit electric charge, i.e. $Q_U - Q_D = 1$, where Q is the electric charge of either the up-type or down-type quirks. The mass ratio squared R_i and the relative velocity $\beta_{i,f}$ appearing in the formulas below are defined as

$$R_i = \frac{m_i^2}{M^2}, \quad \text{and} \quad (B1)$$

$$\beta_{i,j} = \sqrt{1 + (R_i - R_j)^2 + 2(R_i + R_j)}, \quad (B2)$$

respectively, and $c_W = \cos \theta_W$ is the cosine of the Weinberg angle.

1. $W^+\gamma$

The charged quirkonium decay widths into $W^+\gamma$ are qualitatively different to the widths of neutral quirkonia into $Z\gamma$. There are two reasons for the differences; the decay into $W^+\gamma$ can go through an s -channel with a W exchange. The corresponding diagram is absent for $Z\gamma$; the photon does not couple to a electrically neutral Z . Another reason is that the photon couples to quirks of different electric charges in the t - and u -channel diagrams, due to the emission of a charged W . It is illuminating to write the chiral projection operators as $P_{L,R} = (v_W \mp a_W \gamma^5)/2$, with $a_W = v_W = 1$, so that the vector and axial-vector contributions from the W current are manifest. The partial widths into $W^+\gamma$ are

$$\Gamma(^1S_0^+ \rightarrow W^+\gamma) = \frac{N\alpha\alpha_W v_W^2}{4M^2} (Q_U + Q_D)^2 (1 - R_W) |R_S(0)|^2, \quad (B3)$$

$$\Gamma(^3S_1^+ \rightarrow W^+\gamma) = \frac{N\alpha\alpha_W a_W^2}{12m_W^2} (Q_U + Q_D)^2 (1 - R_W^2) |R_S(0)|^2, \quad (B4)$$

$$\Gamma(^1P_1^+ \rightarrow W^+\gamma) = \frac{N\alpha\alpha_W}{M^2 m_W^2} [a_W^2 (Q_U + Q_D)^2 (1 - R_W^2) + v_W^2 (Q_U - Q_D)^2 R_W (1 - R_W)] |R'_P(0)|^2, \quad (B5)$$

$$\Gamma(^3P_0^+ \rightarrow W^+\gamma) = \frac{N\alpha\alpha_W (1 - R_W)}{M^4} \left[a_W^2 (Q_U - Q_D)^2 + v_W^2 (Q_U + Q_D)^2 \left(1 + \frac{2}{1 - R_W} \right)^2 \right] |R'_P(0)|^2, \quad (B6)$$

$$\Gamma(^3P_1^+ \rightarrow W^+\gamma) = \frac{N\alpha\alpha_W}{2M^2 m_W^2} \left[a_W^2 (1 - R_W) + 4v_W^2 (Q_U + Q_D)^2 R_W \frac{1 + R_W}{1 - R_W} \right] |R'_P(0)|^2, \quad (B7)$$

$$\Gamma(^3P_2^+ \rightarrow W^+\gamma) = \frac{N\alpha\alpha_W (1 - R_W)}{10M^2 m_W^2} \left[a_W^2 (Q_U - Q_D)^2 (3 + 4R_W) + \frac{4v_W^2 (Q_U + Q_D)^2 R_W (6 + 3R_W + R_W^2)}{(1 - R_W)^2} \right] |R'_P(0)|^2. \quad (B8)$$

Interestingly, all but one term in $\Gamma(^3P_1^+ \rightarrow W^+\gamma)$ are proportional to either the hypercharge $Y = (Q_U + Q_D)/2$ or the isospin $T_{3U} = (Q_U - Q_D)/2$ of the quirks.

2. W^+H

In the limit degenerate quirk masses, their coupling constants to the Higgs boson are the same. As a consequence, the decay matrix elements has the same form as that for the decay into ZH , and can be obtained by the replacements

² We found a relative sign difference between the two terms in the amplitude $A(^3P_1)$. We attribute this to our definition of $\epsilon^{0123} = 1$.

$g_Z \rightarrow g/\sqrt{2}$ and vector and axial vector couplings by $1/2$; $a, v \rightarrow 1/2$. This gives a conversion factor of $1/(2\sqrt{2})$ converting the ZH matrix elements to WH :

$$\mathcal{M}_{W^+H} = \frac{1}{2\sqrt{2}} \mathcal{M}_{ZH}. \quad (\text{B9})$$

Therefore, the partial widths into W^+H , have exactly the same form as those for ZH , aside from a factor of $1/8$. The analysis for ZH in [19] applies to W^+H as well. The partial widths are

$$\Gamma(^1S_0^+ \rightarrow W^+H) = \frac{N\alpha_W^2\beta_{WH}^3}{32M^2} \frac{1}{R_W^2} |R_S(0)|^2, \quad (\text{B10})$$

$$\begin{aligned} \Gamma(^3S_1^+ \rightarrow W^+H) = & \frac{N\alpha_W^2\beta_{WH}}{384} \frac{M^2}{m_W^4} \left(\frac{8R_W[(1-R_W)^2 + R_H(1-3R_W)]^2}{(1-R_W)^2(1-R_H-R_W)^2} \right. \\ & \left. + \frac{[R_H^2(1-3R_W) - 2R_H(1-R_W(2+R_W)) + (1-R_W)(1-R_W^2 - \beta_{WH}^2)]^2}{(1-R_W)^2(1-R_H-R_W)^2} \right) |R_S(0)|^2, \end{aligned} \quad (\text{B11})$$

$$\Gamma(^1P_1^+ \rightarrow W^+H) = \frac{N\alpha_W^2\beta_{WH}^3}{4M^2m_W^2(1-R_H-R_W)^2} |R'_P(0)|^2, \quad (\text{B12})$$

$$\Gamma(^3P_0^+ \rightarrow W^+H) = 0, \quad (\text{B13})$$

$$\begin{aligned} \Gamma(^3P_1^+ \rightarrow W^+H) = & \frac{N\alpha_W^2\beta_{WH}}{8m_W^4} \left(\frac{2[1-R_H+R_W]^2[1+R_W(2-R_H+R_W)]^2}{(1-R_H-R_W)^2(1-R_W)^2} \right. \\ & \left. + R_W \left[\frac{4R_W}{1-R_W} + \frac{\beta_{WH}^2 - 4(1-R_H-R_W)}{(1-R_H-R_W)^2} \right]^2 \right) |R'_P(0)|^2, \end{aligned} \quad (\text{B14})$$

$$\Gamma(^3P_2^+ \rightarrow W^+H) = \frac{3N\alpha_W^2\beta_{WH}^5}{40M^2m_W^2(1-R_H-R_W)^4} |R'_P(0)|^2. \quad (\text{B15})$$

3. WZ

Notice that double longitudinal modes are allowed from the decay of a charged quirkonium in the 1S_0 state. This is impossible for the neutral quirkonium case, where it decays into ZZ or WW . To see this, the 1S_0 state has $J^{PC} = 0^{-+}$, but at zero angular momentum, the double longitudinal state has $J^{PC} = 0^{++}$. The decay into double longitudinal modes for neutral quirkonia in 1S_0 is forbidden by CP conservation. For charged states, the charge parity is irrelevant, and the decay into double longitudinal mode is allowed by CP conservation. Naively, one would expect the 1S_0 decay rate is longitudinal from appearance of the $1/(R_Z R_W)$ term. However, due to the Goldstone s-exchange, at large quirkonium mass M the decay rate vanishes.

$$\Gamma(^1S_0^+ \rightarrow W^+ Z) = \frac{N\alpha_W\alpha_Z\beta_{WZ}}{32M^2} \left(1 - \frac{c_W^2 R_Z}{R_W} \frac{1}{1 + R_W - R_Z}\right)^2 \left(\frac{8}{(1 - R_W - R_Z)^2} + \frac{1}{R_W R_Z}\right) |R_S(0)|^2, \quad (\text{B16})$$

$$\begin{aligned} \Gamma(^3S_1^+ \rightarrow W^+ Z) = & \frac{N\alpha_W\alpha_Z\beta_{WZ}^3}{64M^2} \frac{1}{(1 - R_W)^2(1 - R_W - R_Z)^2} \left\{ 8c_W^4 R_Z^2 \right. \\ & + 2(1 - R_W - 2c_W^2 R_Z)^2 \left(\frac{1}{R_W} + \frac{1}{R_Z}\right) \\ & \left. + \frac{1}{R_W R_Z} (1 - R_W - c_W^2 R_Z(1 + R_W + R_Z))^2 \right\} |R_S(0)|^2, \end{aligned} \quad (\text{B17})$$

$$\begin{aligned} \Gamma(^1P_1^+ \rightarrow W^+ Z) = & \frac{N\alpha_W\alpha_Z\beta_{WZ}}{4M^4(1 - R_W - R_Z)^2} \left\{ \frac{(1 + R_W - R_Z)^2}{R_W} + \frac{(1 - R_W + R_Z)^2}{R_Z} \right. \\ & \left. + 4\left(1 - \frac{c_W^2 \beta_{WZ}^2}{1 - R_W - R_Z}\right)^2 \right\} |R'_P(0)|^2, \end{aligned} \quad (\text{B18})$$

$$\Gamma(^3P_0^+ \rightarrow W^+ Z) = \frac{N\alpha_W\alpha_Z\beta_{WZ}^3}{M^4(1 - R_W - R_Z)^4} [1 - c_W^2(1 - R_W + R_Z)]^2 |R'_P(0)|^2, \quad (\text{B19})$$

$$\begin{aligned} \Gamma(^3P_1^+ \rightarrow W^+ Z) = & \frac{N\alpha_W\alpha_Z\beta_{WZ}^3}{16M^4(1 - R_W - R_Z)^2} \left\{ \frac{32c_W^4 R_Z^2}{(1 - R_W)^2} \right. \\ & + \frac{2}{R_Z} \left[1 + \frac{2R_Z}{1 - R_W - R_Z} - \frac{8c_W^2 R_Z (1 - \frac{R_Z}{2(1 - R_W)})}{1 - R_W - R_Z} \right]^2 \\ & + \frac{2}{R_W} \left[2c_W^4 R_Z \left(1 + \frac{2R_W + R_Z}{1 - R_W}\right)^2 + \left(1 + \frac{2R_W}{1 - R_W - R_Z} - 2c_W^2 \left(1 - \frac{2R_Z}{1 - R_W}\right)\right)^2 \right] \\ & \left. \right\} |R'_P(0)|^2 \end{aligned} \quad (\text{B20})$$

$$\begin{aligned} \Gamma(^3P_2^+ \rightarrow W^+ Z) = & \frac{N\alpha_W\alpha_Z\beta_{WZ}^3}{40M^4(1 - R_W - R_Z)^4} \left\{ 16[1 - c_W^2(1 - R_W + R_Z)]^2 \right. \\ & + \frac{3}{R_Z} [1 - R_W + R_Z - 4c_W^2 R_Z]^2 \\ & \left. + \frac{3}{R_W} [1 + R_W - R_Z - 2c_W^2(1 - R_W - R_Z)]^2 \right\} |R'_P(0)|^2. \end{aligned} \quad (\text{B21})$$

4. $f_u \bar{f}_d$

Decays into two fermions only proceed via the s -channel exchange of W^+ . The non-zero widths with outgoing fermion masses $m_{1,2}$ are

$$\Gamma(^1S_0^+ \rightarrow u\bar{d}) = \frac{N\alpha_W^2\beta_{ud}}{16M^2} \frac{(R_1 - R_1^2 + R_2 + 2R_1 R_2 - R_2^2)}{R_W^2} |R_S(0)|^2, \quad (\text{B22})$$

$$\Gamma(^3S_1^+ \rightarrow u\bar{d}) = \frac{N\alpha_W^2\beta_{ud}}{48M^2} \frac{2 - R_1 - R_1^2 - R_2 + 2R_1 R_2 - R_2^2}{(1 - R_W)^2} |R_S(0)|^2, \quad (\text{B23})$$

$$\Gamma(^3P_1^+ \rightarrow u\bar{d}) = \frac{N\alpha_W^2\beta_{ud}}{2M^4} \frac{2 - R_1 - R_1^2 - R_2 + 2R_1 R_2 - R_2^2}{(1 - R_W)^2} |R'_P(0)|^2. \quad (\text{B24})$$

As expected, the 1S_0 partial width is proportional to m_f^2/M^2 , corresponding to a chirality flip on the outgoing fermion line.

Appendix C: Decay Rates of Neutral Quirkonia

This section summarizes the decay rates of neutral quirkonia. The decay rates differ with [19] by just a factor of 2/3 due to a different color group. We also attempt to rewrite the decay rates so that the origins of the terms in the expression are manifest. In the expressions below, a t -channel quirk exchange with outgoing particles i and j corresponds to the factor $(1 - R_i - R_j)^{-1}$, with $R_i = m_i^2/M^2$, and M is the quirkonium mass. An s -channel diagram exchanging particle ϕ corresponds to $(1 - R_\phi)^{-1}$.

1. $f\bar{f}$

The decays into a fermion-antifermion pair, only the s -channel γ, Z and Higgs diagram contribute. The decay of the 1S_0 state requires a chirality flip on the outgoing fermion line, resulting in the dependence on the fermion mass squared, M_f^2 , in its decay rate - similar to pseudoscalar decay.

$$\Gamma(^1S_0 \rightarrow f\bar{f}) = 8N\alpha_Z^2 a_f^2 a_Q^2 \beta_f \frac{m_f^2}{m_Z^4} |R_S(0)|^2, \quad (C1)$$

$$\Gamma(^3S_1 \rightarrow f\bar{f}) = \frac{4N\alpha_{EM}^2 \beta_f}{3M^2} \left\{ (1 + 2R_f) \left(e_Q e_f + \frac{v_f v_Q}{c_W^2 s_W^2 (1 - R_Z)} \right)^2 + \frac{a_f^2 v_Q^2 \beta_f^2}{c_W^4 s_W^4 (1 - R_Z)^2} \right\} |R_S(0)|^2, \quad (C2)$$

$$\Gamma(^1P_1 \rightarrow f\bar{f}) = 0, \quad (C3)$$

$$\Gamma(^3P_0 \rightarrow f\bar{f}) = \frac{9N\alpha_Z^2 \beta_f^3}{8M^2(1 - R_H)^2} \frac{m_f^2}{m_Z^4} |R'_P(0)|^2, \quad (C4)$$

$$\Gamma(^3P_1 \rightarrow f\bar{f}) = \frac{32N\alpha_Z^2 a_Q^2 \beta_f}{M^4(1 - R_Z)^2} [a_f^2 \beta_f^2 + (1 + 2R_f)v_f^2] |R'_P(0)|^2, \quad (C5)$$

$$\Gamma(^3P_2 \rightarrow f\bar{f}) = 0, \quad (C6)$$

where M is the quirkonium mass, $\alpha_Z = \alpha_{EM}/(c_W^2 s_W^2)$, c_W and s_W are the cosine and sine of the Weinberg angle, respectively, $a_i = T_{3i}/2$ and $v_i = a_i - e_i s_W^2$ are the axial-vector and vector couplings of the Z to fermion i , with $i = \{Q, f\}$ for the quirk and the outgoing fermion, respectively, $R_j = m_j^2/M^2$, and $\beta_f = \sqrt{1 - 4R_f}$ is the relative velocity between the two outgoing fermions.

2. $Z\gamma$

Only the t -channel diagram contributes decays into $Z\gamma$,

$$\Gamma(^1S_0 \rightarrow Z\gamma) = \frac{8N\alpha_{EM}\alpha_Z e_Q^2 v_Q^2}{M^2} (1 - R_Z) |R_S(0)|^2, \quad (C7)$$

$$\Gamma(^3S_1 \rightarrow Z\gamma) = \frac{8N\alpha_{EM}\alpha_Z e_Q^2 a_Q^2}{3m_Z^2} (1 - R_Z^2) |R_S(0)|^2, \quad (C8)$$

$$\Gamma(^1P_1 \rightarrow Z\gamma) = \frac{32N\alpha_{EM}\alpha_Z e_Q^2 a_Q^2}{M^2 m_Z^2} (1 - R_Z^2) |R'_P(0)|^2, \quad (C9)$$

$$\Gamma(^3P_0 \rightarrow Z\gamma) = \frac{32N\alpha_{EM}\alpha_Z e_Q^2 v_Q^2}{M^4(1 - R_Z)} (3 - R_Z)^2 |R'_P(0)|^2, \quad (C10)$$

$$\Gamma(^3P_1 \rightarrow Z\gamma) = \frac{64N\alpha_{EM}\alpha_Z e_Q^2 v_Q^2}{M^2 m_Z^2 (1 - R_Z)} (1 + R_Z) R_Z^2 |R'_P(0)|^2, \quad (C11)$$

$$\Gamma(^3P_2 \rightarrow Z\gamma) = \frac{64N\alpha_{EM}\alpha_Z e_Q^2 v_Q^2}{5M^2 m_Z^2 (1 - R_Z)} (R_Z^2 + 3R_Z + 6) |R'_P(0)|^2, \quad (C12)$$

where the definitions of various quantities can be found in the paragraph below Eq. (C6).

3. W^+W^-

$$\Gamma(^1S_0 \rightarrow W^+W^-) = \frac{N\alpha_W^2\beta_W^3}{8M^2(1-2R_W)^2}|R_S(0)|^2, \quad (C13)$$

$$\begin{aligned} \Gamma(^3S_1 \rightarrow W^+W^-) = & \frac{NM^2\alpha_W^2\beta_W^3}{48m_W^4} \left\{ \frac{R_W(2-R_W)}{(1-2R_W)^2} - \frac{4R_W(5+6R_W)}{1-2R_W} \left(e_Q s_W^2 + \frac{v_Q}{1-R_Z} \right) \right. \\ & \left. + 4(1+20R_W+12R_W^2) \left(e_Q s_W^2 + \frac{v_Q}{1-R_Z} \right)^2 \right\} |R_S(0)|^2, \end{aligned} \quad (C14)$$

$$\Gamma(^1P_1 \rightarrow W^+W^-) = \frac{3N\alpha_W^2\beta_W}{8M^2m_W^2(1-2R_W)^2} \left\{ 1 + \beta_W^2 + 2R_W \left(1 + \frac{\beta_W^2}{1-2R_W} \right)^2 \right\} |R'_P(0)|^2, \quad (C15)$$

$$\begin{aligned} \Gamma(^3P_0 \rightarrow W^+W^-) = & \frac{N\alpha_W^2\beta_W}{4m_W^4} \left\{ \left[\frac{1}{1-2R_W} \left(1 - 3R_W + \frac{\beta_W^2 R_W}{1-2R_W} \right) - \frac{3}{1-R_H} \left(\frac{1}{2} - R_W \right) \right]^2 \right. \\ & \left. + 2R_W^2 \left[\frac{1}{1-2R_W} \left(1 - \frac{\beta_W^2}{1-2R_W} \right) - \frac{3}{1-R_H} \right]^2 \right\} |R'_P(0)|^2, \end{aligned} \quad (C16)$$

$$\begin{aligned} \Gamma(^3P_1 \rightarrow W^+W^-) = & \frac{N\alpha_W^2\beta_W^3}{32m_W^2} \left\{ [32R_W^2 + (3 - \beta_W^2)]^2 \left(\frac{1}{1-2R_W} - \frac{1}{1-R_Z} \right)^2 \right. \\ & \left. + 4R_W \left[\left(\frac{3-4R_W}{(1-2R_W)^2} - \frac{4}{1-R_Z} \right)^2 + \frac{\beta_W^4}{(1-2R_W)^4} \right] \right\} |R'_P(0)|^2, \end{aligned} \quad (C17)$$

$$\begin{aligned} \Gamma(^3P_2 \rightarrow W^+W^-) = & \frac{N\alpha_W^2\beta_W}{40m_W^4(1-2R_W)^2} \left\{ \left(1 - \frac{2R_W\beta_W^2}{1-2R_W} \right)^2 \right. \\ & + 6R_W \left[1 - \frac{2R_W\beta_W^4}{(1-2R_W)^2} + \left(1 - \frac{\beta_W^2}{1-2R_W} \right)^2 \right] \\ & \left. + 8R_W^2 \left[6 + \left(1 - \frac{\beta_W^2}{1-2R_W} \right)^2 \right] \right\} |R'_P(0)|^2, \end{aligned} \quad (C18)$$

where $\alpha_W = \alpha_{EM}/s_W^2$, $\beta_W = \sqrt{1-4R_W}$ is the relative velocity of the two W 's, e_Q, v_Q , and a_Q are the electric charge, vector and axial-vector couplings to the Z of the quirk, respectively, and $R_W = m_W^2/M^2$.

4. ZZ

$$\Gamma(^1S_0 \rightarrow ZZ) = \frac{4N(a_Q^2 + v_Q^2)\alpha_Z^2\beta_Z^3}{M^2(1-2R_Z)^2}|R_S(0)|^2, \quad (C19)$$

$$\Gamma(^3S_1 \rightarrow ZZ) = \frac{8Na_Q^2v_Q^2\alpha_Z^2\beta_Z^5}{3m_Z^2(1-2R_Z)^2}|R_S(0)|^2, \quad (C20)$$

$$\Gamma(^1P_1 \rightarrow ZZ) = \frac{32Na_Q^2v_Q^2\alpha_Z^2\beta_Z^3}{M^2m_Z^2(1-2R_Z)^2}|R'_P(0)|^2, \quad (C21)$$

$$\begin{aligned} \Gamma(^3P_0 \rightarrow ZZ) = & \frac{N\alpha_Z^2\beta_Z}{32m_Z^4} \left\{ \left(32a_Q^2 - \frac{3-6R_Z}{1-R_H} - \frac{64R_Z^2v_Q^2}{(1-2R_Z)^2} \right)^2 \right. \\ & \left. + 8R_Z^2 \left(\frac{3}{1-R_H} - \frac{32R_Zv_Q^2}{(1-2R_Z)^2} - \frac{8(3-4R_Z)(a_Q^2 - v_Q^2)}{(1-2R_Z)^2} \right)^2 \right\} |R'_P(0)|^2, \end{aligned} \quad (C22)$$

$$\Gamma(^3P_1 \rightarrow ZZ) = \frac{16N\alpha_Z^2\beta_Z^5}{M^2m_Z^2(1-2R_Z)^2} \left(\frac{2R_Zv_Q^2}{1-2R_Z} - a_Q^2 \right)^2 |R'_P(0)|^2, \quad (C23)$$

$$\begin{aligned} \Gamma(^3P_2 \rightarrow ZZ) = & \frac{16N\alpha_Z^2\beta_Z}{5m_Z^4} \left\{ \left(a_Q^2 + v_Q^2 \frac{4R_Z^2}{(1-2R_Z)^2} \right)^2 + \frac{3R_Z}{(1-2R_Z)^2} \left(a_Q^2 + v_Q^2 \frac{2R_Z}{1-2R_Z} \right)^2 \right. \\ & \left. + (v_Q^2 + a_Q^2)^2 \frac{4R_Z^2}{(1-2R_Z)^2} \left(3 + \frac{2R_Z^2}{(1-2R_Z)^2} \right) \right\} |R'_P(0)|^2, \end{aligned} \quad (C24)$$

where $\beta_Z = \sqrt{1-4R_Z}$ is the relative velocity between the Z 's. The definitions of other quantities can be found below Eq. (C6).

5. ZH

$$\Gamma(^1S_0 \rightarrow ZH) = \frac{N\alpha_Z^2 a_Q^2 M^2 \beta_{ZH}^3}{4m_Z^4} |R_S(0)|^2, \quad (C25)$$

$$\Gamma(^3S_1 \rightarrow ZH) = \frac{N\alpha_Z^2 v_Q^2 \beta_{ZH}}{6m_Z^2} \left\{ \left(\frac{1-R_H+R_Z}{1-R_H-R_Z} - \frac{2R_Z}{1-R_Z} \right)^2 + \frac{R_Z}{2} \left(\frac{1-R_H+R_Z}{1-R_Z} - \frac{2}{1-R_H-R_Z} \right)^2 \right\} |R_S(0)|^2, \quad (C26)$$

$$\Gamma(^1P_1 \rightarrow ZH) = \frac{2Nv_Q^2 \alpha_Z^2 \beta_{ZH}^3}{M^2 m_Z^2 (1-R_H-R_Z)^2} |R'_P(0)|^2, \quad (C27)$$

$$\Gamma(^3P_0 \rightarrow ZH) = 0, \quad (C28)$$

$$\Gamma(^3P_1 \rightarrow ZH) = \frac{2Na_Q^2 \alpha_Z^2 \beta_{ZH}}{m_Z^4} \left\{ (1-R_H+R_Z)^2 \left(\frac{R_Z}{1-R_Z} - \frac{1}{1-R_H-R_Z} \right)^2 + 8R_Z \left(\frac{R_Z}{1-R_Z} - \frac{1}{1-R_H-R_Z} - \frac{\beta_{ZH}^2}{4(1-R_H-R_Z)^2} \right)^2 \right\} |R'_P(0)|^2, \quad (C29)$$

$$\Gamma(^3P_2 \rightarrow ZH) = \frac{3Na_Q^2 \alpha_Z^2 \beta_{ZH}^5}{5M^2 m_Z^2 (1-R_H-R_Z)^4} |R'_P(0)|^2, \quad (C30)$$

6. γH

$$\Gamma(^3S_1 \rightarrow \gamma H) = \frac{Ne_Q^2 \alpha_{EM} \alpha_Z (1-R_H)}{6m_Z^2} |R_S(0)|^2, \quad (C31)$$

$$\Gamma(^1P_1 \rightarrow \gamma H) = \frac{2Ne_Q^2 \alpha_{EM} \alpha_Z (1-R_H)}{M^2 m_Z^2} |R'_P(0)|^2, \quad (C32)$$

$$(C33)$$

7. HH

$$\Gamma(^3P_0 \rightarrow HH) = \frac{N\alpha_Z^2 \beta_H}{32m_Z^4} \left(\frac{9R_H}{1-R_H} - \frac{6}{1-2R_H} + \frac{\beta_H^2}{(1-2R_H)^2} \right)^2 |R'_P(0)|^2, \quad (C34)$$

$$\Gamma(^3P_2 \rightarrow HH) = \frac{N\alpha_Z^2 \beta_H^5}{80m_Z^4 (1-2R_H)^4} |R'_P(0)|^2. \quad (C35)$$

-
- [1] J. Kang and M. A. Luty, JHEP **0911**, 065 (2009) [arXiv:0805.4642 [hep-ph]].
 - [2] L. B. Okun, JETP Lett. **31**, 144 (1980) [Pisma Zh. Eksp. Teor. Fiz. **31**, 156 (1979)]; L. B. Okun, Nucl. Phys. B **173**, 1 (1980); J. D. Bjorken, (1979), SLAC-PUB-2372; S. Gupta and H. R. Quinn, Phys. Rev. D **25**, 838 (1982).
 - [3] G. Burdman, Z. Chacko, H. S. Goh, R. Harnik and C. A. Krenke, Phys. Rev. D **78**, 075028 (2008) [arXiv:0805.4667 [hep-ph]].
 - [4] K. Cheung, W. -Y. Keung, T. -C. Yuan, Nucl. Phys. **B811**, 274-287 (2009). [arXiv:0810.1524 [hep-ph]].
 - [5] R. Harnik, T. Wizansky, Phys. Rev. **D80**, 075015 (2009). [arXiv:0810.3948 [hep-ph]].
 - [6] H. Cai, H. -C. Cheng, J. Terning, JHEP **0905**, 045 (2009). [arXiv:0812.0843 [hep-ph]].
 - [7] C. Kilic, T. Okui, R. Sundrum, JHEP **1002**, 018 (2010). [arXiv:0906.0577 [hep-ph]].
 - [8] S. Chang, M. A. Luty, [arXiv:0906.5013 [hep-ph]].
 - [9] S. Nussinov and C. Jacoby, arXiv:0907.4932 [hep-ph].
 - [10] G. D. Kribs, T. S. Roy, J. Terning, K. M. Zurek, Phys. Rev. **D81**, 095001 (2010). [arXiv:0909.2034 [hep-ph]].
 - [11] C. Kilic, T. Okui, JHEP **1004**, 128 (2010). [arXiv:1001.4526 [hep-ph]].

- [12] L. Carloni and T. Sjostrand, JHEP **1009**, 105 (2010) [arXiv:1006.2911 [hep-ph]].
- [13] S. P. Martin, Phys. Rev. **D83**, 035019 (2011). [arXiv:1012.2072 [hep-ph]].
- [14] R. Harnik, G. D. Kribs and A. Martin, arXiv:1106.2569 [hep-ph].
- [15] M. J. Strassler, K. M. Zurek, Phys. Lett. **B651**, 374-379 (2007). [hep-ph/0604261].
- [16] T. Han, Z. Si, K. M. Zurek, M. J. Strassler, JHEP **0807**, 008 (2008). [arXiv:0712.2041 [hep-ph]].
- [17] M. J. Strassler, [arXiv:0806.2385 [hep-ph]].
- [18] V. M. Abazov *et al.* [D0 Collaboration], Phys. Rev. Lett. **105**, 211803 (2010). [arXiv:1008.3547 [hep-ex]].
- [19] V. D. Barger, E. W. N. Glover, K. Hikasa, W. Y. Keung, M. G. Olsson, C. J. . Suchyta and X. R. Tata, Phys. Rev. D **35**, 3366 (1987) [Erratum-ibid. D **38**, 1632 (1988)].
- [20] B. Guberina, J. H. Kuhn, R. D. Peccei and R. Ruckl, Nucl. Phys. B **174**, 317 (1980).
- [21] T. Aaltonen *et al.* [CDF Collaboration], arXiv:1104.0699 [hep-ex].
- [22] A. Annovi, P. Catastini, V. Cavaliere, and L. Ristori, http://www-cdf.fnal.gov/physics/ewk/2011/wjj/7_3.html.